
DIFFUSION-BASED AUDIO INPAINTING*

Eloi Moliner, Vesa Välimäki

Acoustics Lab

Department of Information and Communications Engineering

Aalto University, Espoo, Finland

eloi.moliner@aalto.fi

ABSTRACT

Audio inpainting aims to reconstruct missing segments in corrupted recordings. Most of existing methods produce plausible reconstructions when the gap lengths are short, but struggle to reconstruct gaps larger than about 100 ms. This paper explores recent advancements in deep learning and, particularly, diffusion models, for the task of audio inpainting. The proposed method uses an unconditionally trained generative model, which can be conditioned in a zero-shot fashion for audio inpainting, and is able to regenerate gaps of any size. An improved deep neural network architecture based on the constant-Q transform, which allows the model to exploit pitch-equivariant symmetries in audio, is also presented. The performance of the proposed algorithm is evaluated through objective and subjective metrics for the task of reconstructing short to mid-sized gaps, up to 300 ms. The results of a formal listening test show that the proposed method delivers comparable performance against the compared baselines for short gaps, such as 50 ms, while retaining a good audio quality and outperforming the baselines for wider gaps that are up to 300 ms long. The method presented in this paper can be applied to restoring sound recordings that suffer from severe local disturbances or dropouts, which must be reconstructed.

1 INTRODUCTION

Audio inpainting refers to repairing or filling in missing or degraded parts of an audio signal [1]. Inpainting can be used to remove noise, glitches, or other unwanted artifacts from an audio recording, or to fill in missing sections of audio that have been lost or damaged. Application examples include the restoration of old recordings corrupted by local disturbances [2, 3], the reconstruction of missing audio samples caused by scratches in CDs [4], or compensation of audio packet losses in communication networks [5]. In addition, audio inpainting can be used in music and audio production to create special effects or to manipulate audio signals in creative ways [6]. This paper presents a novel audio inpainting method based on the recently proposed diffusion model [7, 8], a deep learning technique capable of generating new content.

Inpainting is necessary when a signal segment is completely missing or it is so severely damaged that noise reduction is impossible and the segment must be deleted and reconstructed. The task of audio inpainting is an ill-posed inverse problem, characterized by a non-unique set of solutions. Audio inpainting has been widely studied in the literature [1, 9, 10, 11, 12]. The methods are characterized by the way the observed signal samples are used as a prior, or pre-existing assumptions about the signal. For instance, some techniques are founded on autoregression [4] or signal sparsity [13]. However, most techniques only work well for gaps of less than 100 ms in length, and start to degrade for longer gaps, or when the assumption of stationarity does not hold.

In this work, we use generative priors, learned from a diffusion probabilistic model, assuming that the solution belongs to the same probability distribution as the dataset used for training. Inpainting methods based on deep generative models can reach new levels of expressivity, as they are not grounded by the stationarity condition and can generate new events in the inpainted gap [14, 15, 16]. In particular, diffusion models have a strong potential to excel on this task as they enjoy a great versatility for solving inverse problems [17, 18, 16].

*Submitted for publication to the Journal of Audio Engineering Society on January 30th, 2023.

In our previous study [16], the invertible Constant-Q Transform (CQT) was used with a diffusion model for solving inverse problems in audio [16]. This paper revisits the use of the CQT, proposing an improved neural network architecture operating in the transform domain using a small amount of signal redundancy. A diffusion model, built with a deep neural network, is first trained with audio material as an unconditional generator. During inference, the model is conditioned in a zero-shot manner to generate a plausible reconstruction of the missing segment. In contrast to existing audio inpainting methods [11, 10, 12], the proposed diffusion model can regenerate gaps of arbitrary length, and retaining high quality for longer gaps.

This paper addresses the inpainting of compact gaps in an audio signal without any accompanying side information. Specifically, we focus on gaps in the short-to-medium size range, ranging from 25 to 300 ms. Note that this differs from the goal of our previous work [16], where the model was tested on larger gaps up to 1.5 s in length. We observed that when the gap was very long, the model had to generate new events. While these generated events were often statistically plausible, they did not align with the musical context and were deemed musically incorrect, which is undesirable. This led us to conclude that a practical inpainting method for large gaps would require a high-level understanding of the music structure or the ability to be conditioned with a guiding signal, as proposed in recent research [19]. However, such considerations fall outside the scope of this paper. As a result, we limit the evaluation to gaps no longer than 300 ms. Within this range, we assume that the content to be filled can be anticipated by a human listener, ensuring a reliable evaluation of the inpainting performance.

The rest of this paper is organized as follows. Sec. 2 reviews the relevant audio and image inpainting literature. Sec. 3 explains the basics of diffusion models and the conditioning method for the inpainting task. Sec. 4 introduces the new diffusion model architecture, which employs the invertible CQT. Sec. 5 compares the proposed method with previous inpainting methods in terms of objective and subjective metrics. Sec. 6 concludes the paper.

2 OVERVIEW OF INPAINTING METHODS

This section reviews some relevant methods in the audio inpainting literature. In addition, we summarize some recent work on image inpainting with diffusion models, which inspired this work.

2.1 Previous Audio Inpainting Methods

Adler et al. first used the term “audio inpainting” to describe the restoration of gaps in audio signals [1], adopting the name from the image inpainting literature. However, this is an old problem in audio processing, and the same task has been previously referred to in the literature as audio interpolation [4, 20, 21] or extrapolation [22, 23], reconstruction of missing samples [24, 25], waveform substitution [5], and imputation [26], among others. The first methods used interpolation techniques based on the observed samples surrounding the gap [4]. A family of successful methods uses autoregressive modeling based on the assumption that the signal is stationary and can be approximated by a linear combination of past samples [4, 20, 21].

A more recent family of methods take advantage of sparse signal representations [13, 10, 9], such as the short-time Fourier transform (STFT). These methods try to find the sparse representation of the missing part of the signal that best fits the surrounding, uncorrupted signal. An established method for enhancing sparsity-based audio inpainting is to learn the dictionary of basis functions. [27, 11]. Another recent work uses non-negative matrix factorization, exploiting the low-rankness of the magnitude spectra as a prior [28].

The methods mentioned above only perform well for inpainting short gaps, roughly in the range from 10 ms to 100 ms. For longer gaps, these methods tend to fail at producing plausible reconstructions as the stationarity condition does not hold true. Some inpainting attempts for long gaps are based on strong assumptions about the underlying structure of the gap, including sinusoidal modeling [29] or similarity graphs [30].

2.2 Deep-Learning Based Audio Inpainting

During the last few years, a new trend has emerged using deep learning based techniques for audio restoration, including several works targeting the task of inpainting. Most of these works use generative models as the prior for inpainting. This allows for methods that are not restricted by the stationarity assumption and are able to generate new content in the gaps to fill in. For instance, Generative Adversarial Networks (GANs) have been explored for this task [14, 15, 31]. Most of these methods are based on a supervised problem-specialized setting, where a dataset of masked/reconstructed audio signals needs to be built to train the model. A shortcoming of using this approach, is that a model that fits the degradations seen during the training does often not generalize to unseen degradations and, as a consequence, lacks the versatility to be applied for restoring gaps of arbitrary lengths.

Some other closely related works fall under the category of packet-loss concealment, which is a similar problem to audio inpainting but with real-time constraints and usually targeting speech signals. Within this context, predictive methods based on convolutional and recurrent neural networks [32, 33] as well as GANs [34, 35] have been proposed.

Also worth mentioning are other recent works that have applied multi-modal side information as a conditioner for the inpainting algorithm, including video frames [36], symbolic music [37, 19], or text [38, 39]. Although this idea falls out of scope of this paper, exploiting multi-modal information may turn out to be beneficial to inpaint large gaps, where the context of the gap does not contain enough information to reconstruct the missing segment.

2.3 Diffusion Models for Image Inpainting

The task of inpainting with generative models has shown a strong impact on image processing research. Relevant to this paper are recent works applying diffusion models for image inpainting. There are two main strategies in the literature for solving inverse problems with diffusion models, including inpainting. The first one consists of sequentially replacing the observed part of the signal in the reverse diffusion process [8, 40]. This idea ensures data consistency and is conceptually simple but, in practice, it struggles at generating consistent content. Other works refined this approach by incorporating ideas that benefited its versatility and performance, such as using singular-value decomposition [17] or resampling multiple times during each sampling step [41]. The other strategy builds on a Bayesian interpretation of posterior sampling and estimates the gradients of the log-likelihood function [18, 42], as elaborated in Sec. 3.2. These methods allow for a good approximation of the posterior distribution, which leads to enhanced inpainting results, at the expense of a higher computational cost.

3 A DIFFUSION MODEL FOR AUDIO INPAINTING

Diffusion models are a class of generative models that have gained a broad interest during recent years for a wide range of modalities, such as images [7, 43, 44], audio [45, 46, 16], video [47], and symbolic music [37], among others. These models generate new data instances by reversing the diffusion process, by which data $\mathbf{x}_0 \sim p_{\text{data}}$ is progressively diffused into Gaussian noise $\mathbf{x}_T \sim \mathcal{N}(\mathbf{0}, \sigma_{\text{max}}^2 \mathbf{I})$ over time τ [7]².

We follow the parameterization by Karras et al. [48], who define the reverse diffusion process with the following *probability flow Ordinary Differential Equation (ODE)*:

$$d\mathbf{x} = -\dot{\sigma}(\tau)\sigma(\tau)\nabla_{\mathbf{x}_\tau} \log p_\tau(\mathbf{x}_\tau)d\tau, \quad (1)$$

where $d\tau$ is an infinitesimal negative timestep, the noise level is defined as $\sigma(\tau) = \tau$, and its first derivative as $\dot{\sigma}(\tau) = 1$. The ODE is governed by the gradient of the log probability density $\nabla_{\mathbf{x}_\tau} \log p_\tau(\mathbf{x}_\tau)$, formally known as the *score* function [49], which can be geometrically interpreted as a vector field pointing towards higher density of data at a given noise level.

The score is analytically intractable but can be approximated as

$$\nabla_{\mathbf{x}_\tau} \log p_\tau(\mathbf{x}_\tau) \approx (D_\theta(\mathbf{x}_\tau, \tau) - \mathbf{x}_\tau)/\sigma(\tau)^2, \quad (2)$$

where $D_\theta(\mathbf{x}_\tau, \tau) = \hat{\mathbf{x}}_0$ is a deep neural network with weights θ , optimized with a denoising euclidean objective. We refer to Karras et al. [48] for further details on the diffusion model formalism and optimization.

In the rest of this section, we elaborate on the audio inpainting problem and the required changes that are applied to the inference process of a diffusion model to solve this task.

3.1 Inverse Problem Formulation

The audio inpainting task can be formulated as a linear inverse problem [1]. Consider an audio signal \mathbf{x}_0 and its observed version \mathbf{y} with missing samples. We can write their relation as

$$\mathbf{y} = \mathbf{m} \odot \mathbf{x}_0, \quad (3)$$

where \mathbf{m} is a binary mask operator and \odot represents the Hadamard product, or element-wise multiplication. In this work, we consider the operator \mathbf{m} as a known compact binary mask, having the value 0 at locations where samples are missing and 1 otherwise. The goal is to recover the original signal \mathbf{x}_0 when the observed measurements \mathbf{y} and mask \mathbf{m} are known.

²The “diffusion time” variable τ must not be confused with the “audio time” t . We use this formulation for notation consistency.

3.2 Audio Inpainting via Posterior Sampling

The iterative nature of diffusion models offers a wide flexibility for solving inverse problems [18, 16]. All that is needed is to substitute the score in Eq. (1) for the *posterior score* $\nabla_{\mathbf{x}} \log p_{\tau}(\mathbf{x}_{\tau}|\mathbf{y})$ [8].

Applying the Bayes’ rule, the posterior factorizes as $p_{\tau}(\mathbf{x}_{\tau}|\mathbf{y}) \propto p_{\tau}(\mathbf{x}_{\tau})p_{\tau}(\mathbf{y}|\mathbf{x}_{\tau})$, which leads to

$$\nabla_{\mathbf{x}_{\tau}} \log p_{\tau}(\mathbf{x}_{\tau}|\mathbf{y}) = \nabla_{\mathbf{x}_{\tau}} \log p_{\tau}(\mathbf{x}_{\tau}) + \nabla_{\mathbf{x}_{\tau}} \log p_{\tau}(\mathbf{y}|\mathbf{x}_{\tau}), \quad (4)$$

where a new term that we refer to as the *noise-perturbed likelihood score* $\nabla_{\mathbf{x}_{\tau}} \log p_{\tau}(\mathbf{y}|\mathbf{x}_{\tau})$ has appeared. Note that this term cannot be derived in closed form due to its dependence of the noise level $\sigma(\tau)$, as \mathbf{x}_{τ} represents the noise-perturbed signal $\mathbf{x}_{\tau} = \mathbf{x}_0 + \sigma(\tau)\epsilon$, where $\epsilon \sim \mathcal{N}(\mathbf{0}, \mathbf{I})$. However, Chung et al. [18] propose to approximate the *noise-perturbed likelihood* with $p_{\tau}(\mathbf{y}|\mathbf{x}_{\tau}) \simeq p(\mathbf{y}|\hat{\mathbf{x}}_0)$, where $\hat{\mathbf{x}}_0$ is the denoised estimate at an intermediate noise level.

Modeling the likelihood as a normal distribution, the *noise-perturbed likelihood score* is approximated as

$$\nabla_{\mathbf{x}_{\tau}} \log p_{\tau}(\mathbf{y}|\mathbf{x}_{\tau}) \simeq -\xi(\tau) \nabla_{\mathbf{x}_{\tau}} \|\mathbf{y} - \mathbf{m} \odot \hat{\mathbf{x}}_0\|^2, \quad (5)$$

This strategy can be understood as a sort of guidance [47], in analogy with classifier guidance [43]. It is important to note that the gradient computation requires differentiating through the neural network F_{θ} , which is responsible for the estimation of $\hat{\mathbf{x}}_0$, resulting in a computational overhead. The variable $\xi(\tau)$ is a scaling function that defines the amount of guidance that is applied during sampling or, in other words, how strongly the conditioning affect the sampling trajectories. We parameterize the scaling function as [16]:

$$\xi(\tau) = \xi' \sqrt{N} / (\sigma(\tau) \|\nabla_{\mathbf{x}_{\tau}} \|\mathbf{y} - \mathbf{m} \odot \hat{\mathbf{x}}_0\|^2\|^2), \quad (6)$$

where N is the length of the audio signal in samples and ξ' is a scalar hyperparameter. Choosing $\xi' = 0$ leads to an unconditional sampler, but selecting too large a value for ξ' results in a degenerate solution. This parameterization normalizes the likelihood gradient by its norm in a similar way as in [50], regularizing the influence of the likelihood throughout the inference process. We empirically observed through qualitative analysis that this strategy allows for robust results.

However, the above conditioning method does not ensure data consistency with the observed samples. When the observed samples \mathbf{y} are noiseless and reliable, as we assume in this work, the preferred solution is to keep them unchanged in the final output. A straightforward way to avoid changing the existing samples is replacing the reliable samples from the intermediate estimates $\hat{\mathbf{x}}_0$ using the inpainting mask. To keep the observed samples, the following data consistency step at each sampling iteration can be applied:

$$\hat{\mathbf{x}}'_0 = \mathbf{y} + (\mathbf{1} - \mathbf{m}) \odot \hat{\mathbf{x}}_0. \quad (7)$$

Although some studies have proved the data consistency step suboptimal [51, 18], other works rely solely on data consistency as a method to condition the diffusion model to solve inverse problems [8, 41]. We observe that applying data consistency steps usually produces discontinuity effects at the boundaries of the mask. To mitigate this effect, we apply a smoothed version of the mask \mathbf{m} for the data consistency step of Eq. (7), which is implemented by fading 1 ms of the reliable signal on the edges of each gap with a raised cosine function.

3.3 Inference

Having defined the probability flow ODE, Eq. (1), and the posterior sampling mechanism, Eq. (5), the next tasks are to discretize and solve the reverse diffusion process, using a trained diffusion model. In this work, we use the second-order stochastic sampler proposed by Karras et al. [48], which offers a good tradeoff between algorithmic complexity and accuracy. This sampler also adds controllable stochasticity into the process, which is intended to regularize approximation errors. The sampling algorithm, specific for inpainting, is described in Algorithm 1. Fig. 1 summarizes graphically the sampling process, omitting the second-order correction for brevity.

As presented in the left-hand side of Fig. 1, the audio signal \mathbf{x}_T is initialized with Gaussian noise, and the noise is iteratively removed throughout the inference process. At each discretization step, we obtain a denoised estimate $\hat{\mathbf{x}}_0$ to which we condition with the input observations (top of Fig. 1) by adding the reconstruction gradient, Eq. (5), and by applying the data consistency step, Eq. (7). Each update step is, practically speaking, a weighted sum of the noisy signal at the given step \mathbf{x}_i and the modified denoised estimate $\hat{\mathbf{x}}'_0$. At the end of the process, shown in the right-hand side of Fig. 1, the noise level becomes imperceptible and, thus, the reconstructed output signal \mathbf{x}_0 is obtained.

The noise schedule represents one of the most critical design choices. Also following [48], given a number of discretization steps T , we define the noise levels as:

$$\tau_{i < T} = \left(\sigma_{\max}^{\frac{1}{\rho}} + \frac{i}{T-1} \left(\sigma_{\min}^{\frac{1}{\rho}} - \sigma_{\max}^{\frac{1}{\rho}} \right) \right)^{\rho}, \quad (8)$$

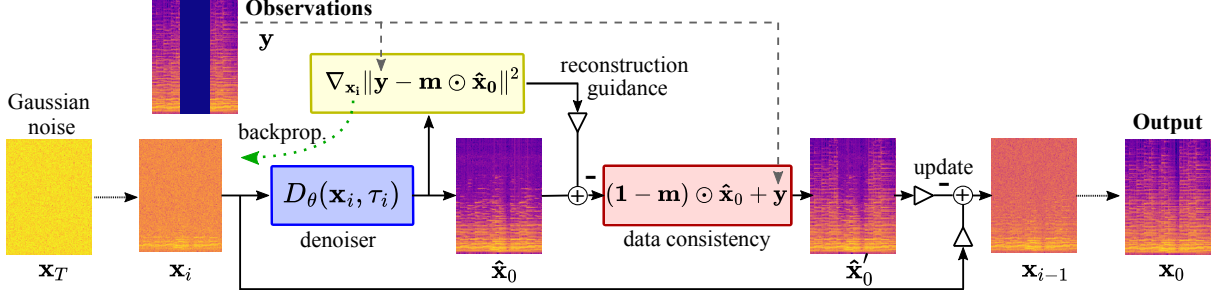


Figure 1: Inference process for audio inpainting in which all straight lines represent a feedforward signal flow in the time domain. The deep neural network is included in the denoiser block. The computation of the reconstruction gradient requires differentiating through the mask and the denoiser block by means of backpropagation, requiring a backward pass through the deep neural network, here illustrated with a green dotted line. The spectrograms are shown for illustrative purposes.

Algorithm 1 Inference Conditioned for Audio Inpainting

Require: observations \mathbf{y} , inpainting mask \mathbf{m} , number of iterations T , noise schedule $\tau_i < T$, stochasticity S_{churn}

Sample $\mathbf{x}_T \sim \mathcal{N}(\mathbf{0}, \sigma_{\text{max}}^2 \mathbf{I})$ ▷ Initial noise is \mathbf{x}_T

$\gamma = \min(S_{\text{churn}}/T, \sqrt{2} - 1)$ ▷ Amount of stochasticity

for $i = T, \dots, 1$ **do** ▷ Step backwards

$\tilde{\tau}_i = \tau_i + \gamma\tau_i$ ▷ Increased noise level

 Sample $\epsilon \sim \mathcal{N}(\mathbf{0}, \mathbf{I})$

$\tilde{\mathbf{x}}_i = \mathbf{x}_i + \sqrt{\sigma(\tilde{\tau}_i)^2 - \sigma(\tau_i)^2} \epsilon$ ▷ Add extra noise

$\hat{\mathbf{x}}_0 = D_\theta(\tilde{\mathbf{x}}_i, \tilde{\tau}_i)$ ▷ Denoiser

$\hat{\mathbf{x}}_0 = H_{\text{post}}(\hat{\mathbf{x}}_0)$ ▷ Post-processing filter

$\hat{\mathbf{x}}_0 = \hat{\mathbf{x}}_0 - \sigma(\tilde{\tau}_i)^2 \xi(\tilde{\tau}_i) \nabla_{\hat{\mathbf{x}}_i} \|\mathbf{y} - \mathbf{m} \odot \hat{\mathbf{x}}_0\|^2$ ▷ Eq. (5)

$\hat{\mathbf{x}}'_0 = \mathbf{y} + (\mathbf{1} - \mathbf{m}) \odot \hat{\mathbf{x}}_0$ ▷ Data consistency

$\mathbf{x}_{i-1} = \tilde{\mathbf{x}}_i - (\sigma(\tau_{i-1}) - \sigma(\tilde{\tau}_i)) \left(\frac{\hat{\mathbf{x}}'_0 - \tilde{\mathbf{x}}_i}{\sigma(\tilde{\tau}_i)} \right)$ ▷ Update step

end for

return \mathbf{x}_0 ▷ Output is the reconstructed signal

where σ_{min} and σ_{max} are, respectively, the minimum and maximum noise levels, i is the discretization index, and ρ is a parameter controlling the warping of the schedule, with higher values of ρ representing more steps at lower noise levels. As in [16], we choose $\sigma_{\text{min}} = 10^{-4}$, $\sigma_{\text{max}} = 1$, and $\rho = 13$. The number of steps T exhibits a clear tradeoff between sample quality and speed. We use the value $T = 70$ in our experiments.

The amount of stochasticity injected into the process is controlled with the S_{churn} parameter [48]. Empirically, we have observed that adding a certain amount of stochasticity helps to producing clean outputs. In our experiments, we choose $S_{\text{churn}} = 10$.

4 IMPROVED CQT-BASED ARCHITECTURE

Diffusion models are architecture agnostic, imposing no constraints on how the neural network F_θ is designed. However, while the choice of architecture does not have theoretical implications, in the best case it can accelerate the convergence of the diffusion model and allow it to produce perceptually-satisfying samples efficiently.

In our previous study [16], we used an invertible CQT [52] to leverage structure from the audio signal and to exploit the pitch-equivariant symmetry that harmonic signals exhibit when they are represented in a logarithmically-spaced time-frequency domain. The most interesting property of the CQT is that a translation on the frequency axis is equivalent to pitch transposition. This symmetry motivates the usage of two-dimensional Convolutional Neural Networks (CNNs), considering that the convolutional operator, which CNNs are composed of, is translation equivariant. In this section, we elaborate the usage of a CQT and introduce an improved neural network architecture that processes audio signals as CQT spectrograms. We call the improved diffusion model based on this architecture the CQT-Diff+ algorithm.

4.1 Using a CQT Representation

The diffusion process described in Sec. 3 is designed in the time domain. However, as part of the computation inside the deep neural network F_θ , the input waveform is represented with an invertible CQT. Concisely, the neural network F_θ is composed as

$$F_\theta = \text{ICQT} \circ F'_\theta \circ \text{CQT}, \quad (9)$$

where CQT and ICQT are, respectively, the constant-Q-transform operation and its inverse, \circ is the function composition operation, and F'_θ refers to the raw neural network layers operating in the transform domain. This approach takes advantage of the structure imposed by the CQT while maintaining maximum versatility. Applying the neural network weights in the transform domain does not impact the optimization, since both the forward transform and its inverse are differentiable.

We use a version of the CQT based on non-stationary Gabor frames [52, 53]. Briefly, this transform is built on a set of K bandpass filters (or Gabor frames) g_k with an equal Q-factor and logarithmically-spaced center frequencies, defined as

$$f_k = f_{\min} 2^{\frac{k-1}{B}}, \quad \text{for } k = 1, 2, 3, \dots, K, \quad (10)$$

where B is the number of bins per octave band (when the number of octave bands is $N_{\text{oct}} = K/B$) and $f_{\min} = f_1$ is the lowest center frequency. The maximum center frequency can be designed to be placed at the Nyquist limit $f_K = f_s/2$. The CQT is applied using the FFT-based processing, as introduced in [52], which allows for an computationally efficient implementation. Further details on the CQT transform and a public repository³ are available elsewhere [52, 53].

4.1.1 Discarding the DC Component

An obvious inconvenience caused by the logarithmic frequency resolution is that there is no DC bin at 0 Hz. If perfect reconstruction is required, one solution is to encode the DC component with a low-pass filter g_{DC} . In our prior work [16], the DC component was included in the model input by concatenating it to the time-frequency matrix. However, we observed the presence of low-frequency artifacts in the generated outputs, which we attribute to the disruption of the logarithmically uniform frequency resolution at the DC component. Therefore, we have made the decision to discard the DC component. By excluding the DC component, the completeness of the CQT as a transform is compromised. The model would now train on only a subset of the transformed space, producing an irreducible error in the frequency bands that it is blind to. However, this issue does not represent a problem in practice, as the audio signals are assumed to be band-limited and, more relevantly, the DC component lies in a frequency range that is imperceptible by the human hearing.

Nevertheless, this irreducible error must be accounted for when propagating the loss during training and, also, during the sampling stage. This can be implemented by applying a post-processing filter to the denoiser output:

$$\hat{x}_0 = H_{\text{post}}(D_\theta(x_\sigma, \sigma)), \quad (11)$$

where H_{post} is a DC notch filter, designed to suppress the frequency range that is not covered by the CQT bandpass filters g_k .

4.1.2 Optimizing Redundancy

In CQTs, the receptive field of the filters decreases geometrically with frequency. In order to guarantee invertibility, the decimation factors of the frequency bands need also to decrease geometrically, producing a non-uniform sampling grid. This feature is not only impractical for constructing a parallelizable and GPU-efficient implementation, but also complicates the architecture design of the neural network. An easy way to overcome this problem is to use instead a CQT with a uniform sampling grid, where the decimation factors remain constant across the frequency range[54]. Previously, this approach allowed treating the CQT as a 2-D matrix, and thus, to directly apply 2-D CNNs [16]. A major drawback of this strategy is its overcompleteness, since the redundancy factor, or the ratio between the number of coefficients in the transformed and original domains, is approximately six [55]⁴. Such a high redundancy factor leads to a suboptimal consumption of memory and computing, as the 2-D CNN is forced to process a substantial amount of signal redundancy. This considerably slowed down the training and inference processes in our previous study [16], and limited the potential scalability of the model.

Schörkhuber et al. [55] proposed to split the CQT into a sequence of octave-wise sub-transforms, each one covering a different octave with a different but constant decimation factor. This strategy allows for a more efficient implementation, as the redundancy factor is reduced to approximately 1.4, a considerable improvement over the matrix version. We

³https://github.com/eloimoliner/CQT_pytorch

⁴The exact value depends on specific transform parameters.

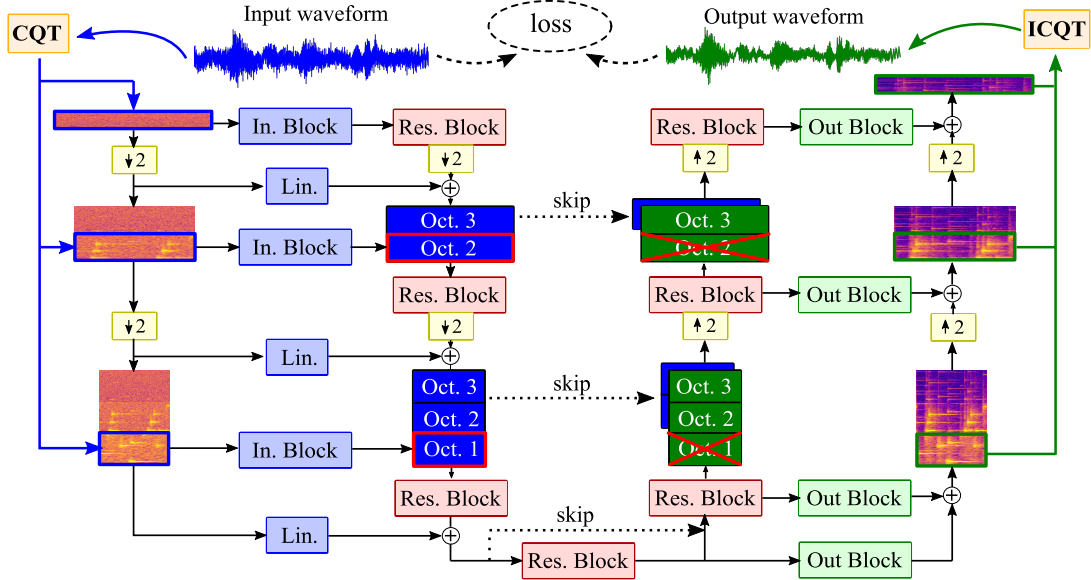


Figure 2: Main diagram of the CQT-U-Net deep neural network architecture. In the diagram, only three octaves out of eight are shown for clarity. The sizes of the spectrograms are not proportional to the real signals.

adopt this strategy, and apply different sub-transforms per each octave band, in our case each of them having 64 frequency bins. A strong advantage of separating the CQT by octave bands is that, when powers of two are used, the time resolution decreases exactly by a factor of two between two consecutive octaves. This choice leads to a hierarchical representation that is suitable to be processed with a U-Net architecture [56].

4.2 Architecture Design

We use a U-Net architecture having a hierarchical encoder/decoder structure, as shown in Fig. 2, where the left-hand side is the encoder and the right-hand side is the decoder. The center part of Fig. 2 is called the “bottleneck”, which corresponds to the lowest point of the letter “U”. The temporal resolution is progressively reduced by a factor of two between consecutive layers in Fig. 2, while the frequency resolution remains unchanged [16]. We make use of this hierarchy by concatenating features from each CQT octave at the U-Net layers where the time resolutions match, as Fig. 2 also illustrates.

The proposed architecture utilizes a double real representation of the complex CQT features, where the real and imaginary parts are stacked as two separate channels. Thus, the real and imaginary part are freely merged in the channel dimension of the network, where the number of channels is further increased, but the synchrony between real and imaginary parts in the time-frequency space is conserved. The chosen strategy aims to circumvent the computational complexity associated with complex-valued layers, as they generally lack empirical performance advantages compared to their real-valued counterparts while imposing higher computational costs [57]. However, even though the neural network views the features as real, the underlying data is complex, and one must be cautious with how the features are processed.

We observed that shift-based operations, such as biases in convolutional layers or mean normalizations, introduced perceptual artifacts to the generated output and, as a consequence, they must be avoided. The intuition behind that lies in the unique nature of complex numbers and the way they interact during computations. In a complex number, the real and imaginary parts represent different dimensions of information. When shift-based operations are applied, they can introduce imbalances between the real and imaginary components, leading to inconsistent phase relationships and distorted information. This does, however, not apply for additive residual connections, as they are designed to add the activations of one layer to another layer without altering their phase relationships. Note that this does not represent a practical limitation to the model as all the signals are zero mean.

In accordance with typical U-Net architectures, concatenative skip connections bridge the intermediate resolutions of the encoder and decoder. An antialiasing filter was used in the downsampling and upsampling layers in the encoder and decoder stages, respectively. At each resolution of both the encoder and the decoder stages and at the bottleneck a residual block (referred to as “Res. Block”) is applied, which constitutes the primary building block of the architecture.

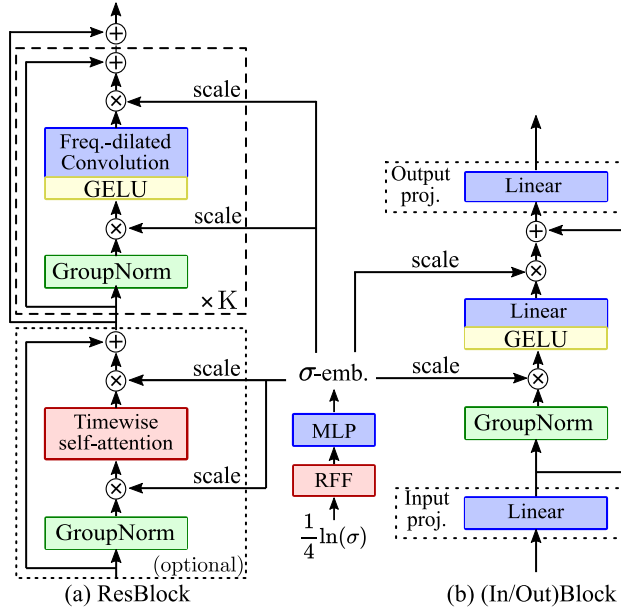


Figure 3: Building blocks of the backbone U-Net architecture, cf. Fig. 2.

In the encoder, the left-hand side of Fig. 2, the input signal is divided into octave-specific “pieces” and processed separately using “In. Blocks”. The features from each octave are then concatenated along the frequency dimension to the corresponding latent vectors of the U-Net at corresponding time resolutions. Additionally, residual connections are applied between the (resized) input features and the corresponding latent vectors of the U-Net to facilitate information flow through all layers of the encoder.

The decoder, or the right-hand side of Fig. 2, comprises of the main signal path that containing “Res. Blocks” and the outer path with residual connections. As the temporal resolution is upsampled in the main path, the features from the lowest octaves at each layer are discarded and projected to the “outer” path via “Out. Blocks.” In the outerpath, at each resolution, the lowest octave is extracted and sent to the ICQT block, as indicated in in Fig. 2. with green lines. This dual-path strategy is inspired by Karras et al. [44], and its purpose is to improve the gradient flow during the optimization process.

The building blocks of Fig. 2 are presented in detail in Fig. 3. They are all conditioned with the noise level embedding σ -emb, which is built with Random Fourier Features (RFF) [58] followed by a Multi-Layer Perceptron (MLP) having three layers. The conditioning is realized by feature-wise linear modulation [59], without shifts. The “In. Block” shown in Fig. 3(b) applies a linear projection to expand the channel size from two (real and imaginary) to the required number of latent features at every layer. They are followed by shift-free Group Normalization, a Gaussian Error Linear Unit (“GELU”) non-linearity, and a linear layer. The “Out. Blocks” have a similar form, but with the linear projection placed at the end, mapping the latent vector to a channel size of two.

Fig. 3(a) shows that each residual block, “Res. Block”, contains a stack of shift-free Group Normalization layers, followed by a “GELU” non-linearity and convolutions in both time and frequency, but with exponentially-increasing dilations in the frequency dimension, meant to provide a wide receptive field while exploiting the symmetry of pitch-equivariance. Optionally, a “Res. Blocks” can contain a timewise self-attention layer, as explained in Sec. 4.2.1.

In contrast to our former work [16], frequency-positional embeddings designed to encode absolute frequency positional information are not used. The reason is that, while the absolute frequencies cannot in principle be retrieved with a CNN, they can in practice be spuriously learned through the use of zero padding [60]. With this modified architecture, zero padding is used in the convolutional layers at each intermediate stage, also in the frequency dimension, propagating absolute positional information throughout the network, even at the shallower layers. We observed that, in this setting, the use of frequency-positional embeddings provided no significant benefit.

4.2.1 Timewise Self-Attention

The motivation behind using timewise self-attention is to allow the model to learn global features through the time dimension, overcoming the locality of CNNs. The use of attention would allow the model to analyze similarities between different segment pairs in time, a feature that could intuitively be highly beneficial for the task of inpainting.

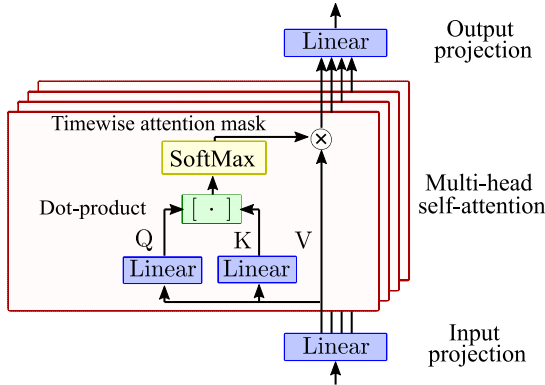


Figure 4: Timewise self-attention block used in Fig. 3.

The latent features are two-dimensional (time and frequency), but since the idea is to apply attention only through time, and not in frequency, this requires some modifications with respect to a basic self-attention mechanism [61].

Fig. 4 presents the functionality of the timewise self-attention block. In order to reduce an unfeasible computational complexity, we introduce a 1×1 convolution before the self-attention mechanism. This reduces the number of channels, which can be quite large (up to 256) to only a few attention heads (set to eight in this work). For each head, the queries Q and keys K are computed with a linear layer, which sees the frequency dimension as the feature dimension. A timewise attention mask is computed via standard dot-product attention, and is later applied to the values V . In order to preserve the structure in the frequency dimension, we do not apply any processing to the values V , apart from the timewise attention. Finally, another 1×1 convolution is applied at the output to expand the reduced number of heads to the original channel size.

4.2.2 Hyperparameter Specification

The architecture of Fig. 2 is designed to work at a sampling frequency of $f_s = 44.1$ kHz. We use a CQT with $B = 64$ bins per octave and $N_{\text{oct}} = 8$ octaves. The depth of the U-Net matches with the number of octaves, and the feature sizes range from 64 at the top U-Net layers to 256 at the bottom. The number of stacked dilated convolutions on each “ResBlock” ranges from two to eight, with fewer dilations at the shallower layers as they need to cover fewer frequency bins and, thus, a large receptive field is not needed. Because of their quadratic complexity, timewise self-attention is only used at the three deepest layers, where the time resolution has been significantly reduced. The total parameter count is 242 million parameters. We refer to the public repository for further specifications⁵.

5 EVALUATION

The performance of the proposed method, which we refer to as CQT-Diff+, is evaluated for inpainting short to middle-sized gaps in musical recordings, ranging from 25 ms to 300 ms.

For comparison, two baselines are considered:

- **LPC**: A method based on signal extrapolation using linear predictive coding [23].
- **A-SPAIN-L**: A sparsity based method for audio inpainting with dictionary learning [11] which is regarded as a state-of-the-art method for short gap inpainting.

Results of both objective and subjective experiments are reported. All experiments use the sample rate of 44.1 kHz. In the objective evaluation, we analyze various gap lengths within intervals of 25 ms.

In the subjective evaluation, we examine four different gap sizes: 50 ms, 100 ms, 200 ms, and 300 ms. In all instances, we intentionally introduce four gaps uniformly across audio segments that have a duration of 4.17 s. These gaps are applied simultaneously at predetermined time locations. Other machine-learning-based methods could not be included in the evaluation, since they were either not designed for wideband music audio [14, 34, 16], or they do not allow enough flexibility to be tested with gaps of different length [12, 15]. For instance, our previous diffusion model [16], which corresponds to a prior iteration of the proposed method, could not be included as a baseline either, because it is unsuitable to work at sample rates higher than 22.05 kHz due to memory constraints.

⁵<https://github.com/eloioliner/audio-inpainting-diffusion/tree/main/conf>

The initial hypothesis is that our method would provide no advantage against the baselines when the gap is very short, as, in this case, stationary conditions can be safely assumed. However, as the duration of the gap increases, the problem gets more challenging and the performance of the baselines is likely to degrade. On the other hand, a diffusion-based generative model should not suffer from this limitation and should be capable of generating audio content regardless of the gap length. Thus, the question we want to resolve is the following: *How does the performance of CQT-Diff+ compare to the baselines in terms of reconstruction quality as the gap length increases?*

5.1 Training

We train our model with the MusicNet dataset, a collection of 330 freely-licensed classical music recordings sampled at 44.1 kHz. MusicNet is a multi-instrument dataset containing recordings from a wide variety of acoustical environments and recording conditions, which represents a challenging and realistic scenario. We use a segment length of 4.17 s, limited by memory requirements. The training is performed using the Adam optimizer, with a learning rate of 2×10^{-4} and a batch size of four. We train the model for roughly 500,000 iterations, which takes approximately five days to train in a single NVIDIA A100 GPU. During training, we track an exponential moving average of the weights, which correspond to the ones used during testing.

5.2 Objective Evaluation

We first conduct an objective evaluation where we report three metrics. The first one is *Log-Spectral Distance* (LSD) [62], a reference-based metric specified as

$$\text{LSD} = \frac{1}{T} \sum_{t=1}^T \sqrt{\frac{1}{K} \sum_{k=1}^K \left(\log |X_{t,k}|^2 - \log |\hat{X}_{t,k}|^2 \right)^2}, \quad (12)$$

where $X_{t,k} = \text{STFT}(\mathbf{x}_0)$ and $\hat{X}_{t,k} = \text{STFT}(\hat{\mathbf{x}}_0)$ are the STFTs of the reference \mathbf{x}_0 and the restored audio signal $\hat{\mathbf{x}}_0$, respectively. For the STFT computation, an analysis window of $K = 2048$ samples and a hop length of 512 samples is used. LSD provides information about the reconstruction performance, with respect to the original signal. Compared to other reference-based metrics such as the signal-to-noise ratio, LSD is less sensible to minor differences as it discards the phase components, aligning better with perception.

We also report the *Objective Difference Grades* (ODG), estimated using the PEMO-Q auditory model [63]. This metric is also reference-based and aims to replicate the subjective difference grades that would be obtained through a subjective listening test. The last metric is *Fréchet Audio Distance* (FAD), which is reference-free, and compares the statistics of a set of generated data against those of a reference dataset [64]. This metric has been demonstrated to correlate with perceptual audio quality [64]. In our case, we compare the distribution of inpainted audio signals with that of the original ones.

The results for different gap lengths are plotted in Fig. 5. For testing, a subset of the MusicNet test set [65] was used, consisting of 60 randomly selected 4.17-s samples, each of them containing four equally-spaced gaps. The test samples were not seen during training the proposed method. The complete test set could not be used due to computational constraints, as processing the entire test set for all the tested conditions would require a large amount of computation.

Fig. 5(a) shows that, according to the LSD metric, for gaps smaller or equal to 100 ms, the proposed method yields a performance similar to the baselines, and marginally outperforms them for longer gaps. The results of the ODG metric are presented in Fig. 5(b), showing how the three compared metrics obtain similar values for small gap lengths, with LPC performing marginally better. Above 100 ms, all the ODG values are below -3 , which we identify to not provide reliable information on the algorithm performance. Finally, Fig. 5(c) shows the FAD results, where lower values (< 5) indicate that the distribution of inpainted audio is statistically similar to the reference. The proposed method consistently achieves a lower FAD values than the compared baselines meaning that the inpainted audio is in-distribution with the rest. Meanwhile, the baselines, in turn, show a strong decline in terms of FAD as the gap size increases.

5.3 Subjective Evaluation

Since there is no guarantee that objective metrics provide reliable information on the perceived quality of the inpainting methods, we conducted a subjective listening experiment. The listening test was designed in accordance with the MUSHRA recommendation [66], using the webMUSHRA evaluation tool [67]. The participants were asked to rate, in a scale from 0 to 100, the perceptual similarity of each item with respect to the reference, which was the original audio sample (without gaps).

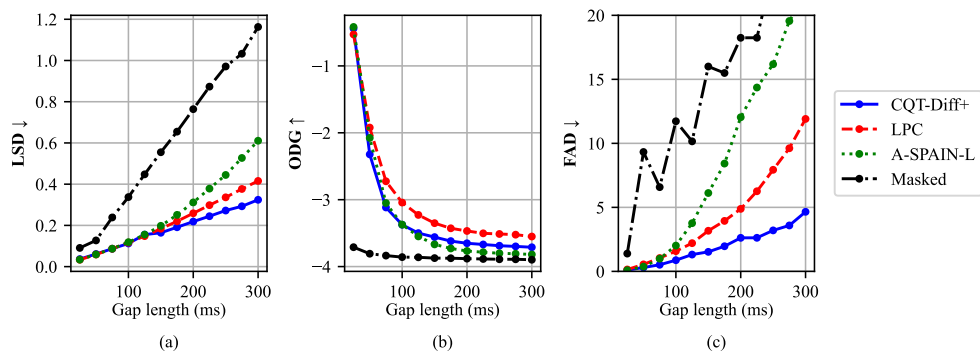


Figure 5: Average objective metrics, including Log-Spectral Distance (LSD), Objective Difference Grades (ODG), and Fréchet Audio Distance (FAD), computed for various gap lengths from 25 to 300 ms. Lower is better for LSD and FAD, while higher is better for ODG. The proposed method (CQT-Diff+) obtained competitive results against the baselines in the reference-based metrics LSD and ODG, while being superior in terms of LSD.

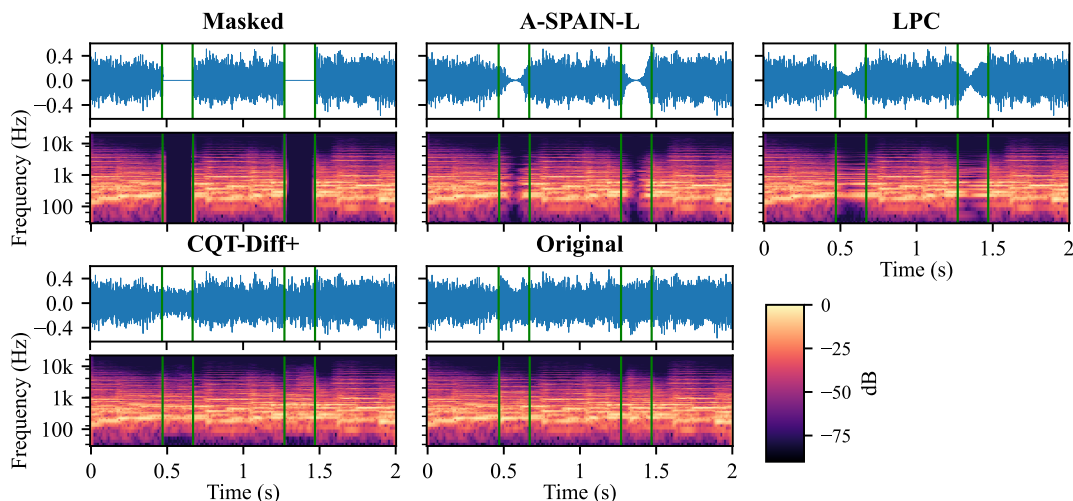


Figure 6: Audio inpainting examples with two gaps of 200 ms, for all five signal types included in the listening test, including waveform and spectrogram representations. The start and end timestamps of the gaps are highlighted with green lines. The original waveform is also included for comparison. The proposed method, CQT-Diff+, produces more coherent and realistic reconstructions than the compared baselines.

The conditions included a low-anchor (a masked version of the reference with four gaps), three reconstructed versions of the low-anchor, produced using the LPC, A-SPAIN-L, and the proposed CQT-Diff+, and a hidden reference (the original unprocessed signal). Fig. 6 show an example of each five conditions with two gaps. The listeners were allowed to loop and focus in detail at the gap locations. The items represented four gap lengths (50, 100, 200, and 300 ms) and 12 randomly-picked 4.17-s examples from the MusicNet test set. The test contained a total of 48 pages of the five items

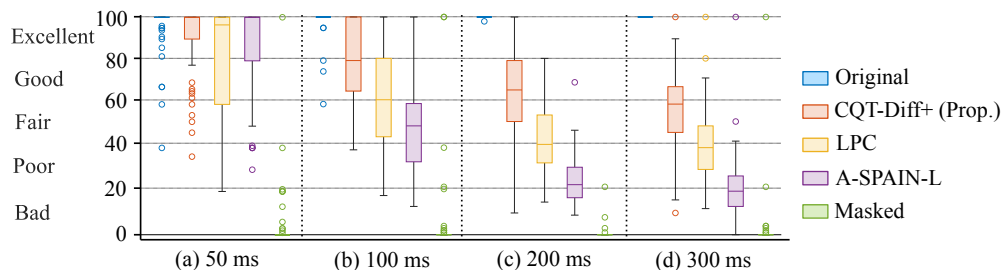


Figure 7: Boxplot diagram of the results of the subjective listening experiment.

above to evaluate. In order to reduce the length of the experiment and avoid listening fatigue, the test was split into two equal-length parts of 24 pages that were alternatively assigned to the participants. A total of 15 volunteers, all without reported hearing defects, participated in the experiment. The average age of the listeners was 28 years old. The audio examples used for the listening test are available at the companion webpage⁶.

The results of the listening test are presented in Fig. 7. Except for 50 ms, when A-SPAIN-L was superior, LPC obtained higher scores than A-SPAIN-L. For the gap length of 50 ms the proposed method obtained similar scores as the compared baselines, all of them skewed towards 100. For the rest of the longer evaluated gaps, the proposed method outperformed the baselines. We study the statistical significance of the score differences between CQT-Diff+ and LPC through a Wilcoxon signed rank test, where we obtain a p-value of 1.2×10^{-4} , 1×10^{-9} , and 3.5×10^{-9} for the gap lengths of 100 ms, 200 ms, and 300 ms, respectively. We conclude that the differences are significant as the p-values are way below 0.05. For all the gap lengths except 50 ms, the results in Fig. 7 show that the proposed method obtain median scores fluctuating between 50 and 80, decreasing proportionally with the gap length. For the shortest gaps of 50 ms, the median score for the proposed CQT-Diff+ method is 100, as the listeners reported to have struggled on finding differences in this test case.

Considering the test question, the listening test result can be interpreted so that the proposed diffusion model performs at least as well as the compared baselines for all gap lengths. The minimum gap length for which the reconstruction using the proposed method is better than the baselines is 100 ms, above that CQT-Diff+ consistently tops the baselines. It can also be concluded that, up to the length of 200 ms, the proposed CQT-Diff+ algorithm produces perceptually “good” audio inpainting (median scores above 60), although distinguishable from the reference in pairwise comparison.

To gain a deeper understanding of the subjective test results, we can qualitatively analyze a specific example depicted in Fig. 6. This figure exhibits waveform and spectrogram representations of a masked music signal (top), along with three reconstructed versions and the original signal (bottom) for reference, all with a gap length of 200 ms. Upon examination, it becomes evident that A-SPAIN-L generates an attenuated reconstruction that fades out towards the middle of the gap and fades in again before reaching the gap’s end. In practice, it shortens the dropout but cannot fill it. The decay observed in the reconstruction arises due to the sparsity penalty, which restricts the generation of content further into the gap. On the other hand, LPC suffers less from this issue as it relies on extrapolation. Nevertheless, this method is only capable of extending stationary sounds and cannot create new attacks and events. Consequently, the reconstructions produced by LPC often sound artificial. Visually, the reconstruction generated with the proposed CQT-Diff+ algorithm fills the gap in a believable manner in Fig. 6. However, a comparison with the original signal shown in the bottom-right pane in Fig. 6 reveals that the reconstruction of the proposed methods is not exact, as the two waveforms look different.

6 CONCLUSION

This paper presents a novel audio inpainting method CQT-Diff+, which is based on recent diffusion models. For the reconstruction of short gaps of 50 ms or less, the proposed method works as well as a previous high-quality inpainting method. For longer gaps, such as 100 ms, 200 ms and 300 ms, the CQT-Diff+ method outperforms the baseline algorithms and retains good quality.

One limitation of the method presented in this paper is that the performance is limited to the types of audio recordings seen during the training, in this case, classical music. To demonstrate the versatility of the proposed approach, we also report, in the form of audio examples in the companion webpage, results obtained with a model trained on a large variety of sound effects. However, these results were excluded from the evaluation in this paper. In the future, the generalizability of the diffusion-based audio inpainting technique should be evaluated by considering models trained on a wider variety of audio recordings.

Another promising direction for future work could involve providing the CQT-Diff+ model with conditional information. In our tests reported elsewhere, a generative method based on a diffusion model created plausible content and new events, when the gaps were 1.5 s long [16]. However, due to the lack of contextual information, the results were difficult to control. A conditional diffusion approach may offer a higher degree of control over the results, especially when dealing with extremely long gaps.

7 ACKNOWLEDGMENT

This research is part of the activities of the Nordic Sound and Music Computing Network (NordForsk project no. 86892). We acknowledge the computational resources provided by the Aalto Science-IT project. We thank the volunteers who participated in the listening test. We are grateful to Luis Costa for proofreading.

⁶<http://research.spa.aalto.fi/publications/papers/jaes-diffusion-inpainting/>

References

- [1] Amir Adler, Valentin Emiya, Maria G Jafari, Michael Elad, Rémi Gribonval, and Mark D Plumbley. Audio inpainting. *IEEE Trans. Audio Speech Lang. Process.*, 20(3):922–932, Mar. 2012.
- [2] Simon J Godsill and Peter JW Rayner. *Digital Audio Restoration*. Springer, 1998.
- [3] Alessandro Ragano, Emmanouil Benetos, and Andrew Hines. Automatic quality assessment of digitized and restored sound archives. *J. Audio Eng. Soc.*, 70(4):252–270, Apr. 2022.
- [4] A. J. E. M. Janssen, R. N. J. Veldhuis, and L. B. Vries. Adaptive interpolation of discrete-time signals that can be modeled as autoregressive processes. *IEEE Trans. Acoust. Speech Signal Process.*, 34(2):317–330, Apr. 1986.
- [5] David Goodman, G Lockhart, O Wasem, and Wai-Choong Wong. Waveform substitution techniques for recovering missing speech segments in packet voice communications. *IEEE Trans. Acoust. Speech Signal Process.*, 34(6):1440–1448, Dec. 1986.
- [6] Théis Bazin, Gaëtan Hadjeres, Philippe Esling, and Mikhail Malt. Spectrogram inpainting for interactive generation of instrument sounds. In *Proceedings of the Joint Conference on AI Music Creativity*, Stockholm, Norway, Jul. 2020.
- [7] Jonathan Ho, Ajay Jain, and Pieter Abbeel. Denoising diffusion probabilistic models. In *Proceedings of NeurIPS*, volume 33, pages 6840–6851, Dec. 2020.
- [8] Yang Song, Jascha Sohl-Dickstein, Diederik P Kingma, Abhishek Kumar, Stefano Ermon, and Ben Poole. Score-based generative modeling through stochastic differential equations. In *Proceedings International Conference on Learning Representations (ICLR)*, May 2021.
- [9] Florian Lieb and Hans-Georg Stark. Audio inpainting: Evaluation of time-frequency representations and structured sparsity approaches. *Signal Process.*, 153:291–299, Dec. 2018.
- [10] Ondřej Mokřý and Pavel Rajmic. Audio inpainting: Revisited and reweighted. *IEEE/ACM Trans. Audio Speech Lang. Process.*, 28:2906–2918, Oct. 2020.
- [11] Georg Tauböck, Shristi Rajbamshi, and Peter Balazs. Dictionary learning for sparse audio inpainting. *IEEE J. Selected Topics Signal Process.*, 15(1):104–119, 2020.
- [12] Andrés Marafioti, Nathanaël Perraudin, Nicki Holighaus, and Piotr Majdak. A context encoder for audio inpainting. *IEEE/ACM Trans. Audio Speech Lang. Process.*, 27(12):2362–2372, 2019.
- [13] Ondřej Mokřý, Pavel Závíška, Pavel Rajmic, and Vítězslav Veselý. Introducing spain (sparse audio inpainter). In *Proceedings of the 27th European Signal Processing Conference (EUSIPCO)*, pages 1–5. IEEE, Sep. 2019.
- [14] Pirmin P Ebner and Amr Eltelt. Audio inpainting with generative adversarial network. *arXiv preprint*, Mar. 2020.
- [15] A. Marafioti, P. Majdak, N. Holighaus, and N. Perraudin. GACELA: A generative adversarial context encoder for long audio inpainting of music. *IEEE J. Selected Topics Signal Process.*, 15(1):120–131, Nov. 2020.
- [16] Eloi Moliner, Jaakko Lehtinen, and Vesa Välimäki. Solving audio inverse problems with a diffusion models. *arXiv preprint*, Oct. 2022.
- [17] Bahjat Kowar, Michael Elad, Stefano Ermon, and Jiaming Song. Denoising diffusion restoration models. In *Proceedings of NeurIPS*, Dec. 2022.
- [18] Hyungjin Chung, Jeongsol Kim, Michael T Mccann, Marc L Klasky, and Jong Chul Ye. Diffusion posterior sampling for general noisy inverse problems. *arXiv preprint*, Nov. 2022.
- [19] Kaiyang Liu, Wendong Gan, and Chenchen Yuan. Maid: A conditional diffusion model for long music audio inpainting. In *Proceedings of the IEEE International Conference on Acoustics, Speech and Signal Processing (ICASSP)*, pages 1–5, Rhodes, Greece, Jun. 2023.
- [20] Walter Etter. Restoration of a discrete-time signal segment by interpolation based on the left-sided and right-sided autoregressive parameters. *IEEE Trans. Signal Processing*, 44(5):1124–1135, 1996.
- [21] Paulo A. A. Esquef, Vesa Välimäki, Kari Roth, and Ismo Kauppinen. Interpolation of long gaps in audio signals using the warped burg’s method. In *Proceedings of the 6th International Conference on Digital Audio Effects (DAFx-03)*, pages 08–11, London, UK, Sep. 2003.
- [22] Ismo Kauppinen, Jyrki Kauppinen, and Pekka Saarinen. A method for long extrapolation of audio signals. *J. Audio Eng. Soc.*, 49(12):1167–1180, Dec. 2001.
- [23] Ismo Kauppinen and Kari Roth. Audio signal extrapolation—theory and applications. In *Proceedings of the International Conference on Digital Audio Effects (DAFx)*, pages 105–110, Hamburg, Germany, Sep. 2002.

- [24] Ismo Kauppinen and Jyrki Kauppinen. Reconstruction method for missing or damaged long portions in audio signal. *J. Audio Eng. Soc.*, 50(7/8):594–602, Jul. 2002.
- [25] P. A. A. Esquef and L. W. P. Biscainho. An efficient model-based multirate method for reconstruction of audio signals across long gaps. *IEEE Trans. Audio Speech Lang. Process.*, 14(4):1391–1400, Jul. 2006.
- [26] Paris Smaragdis, Bhiksha Raj, and Madhusudana Shashanka. Missing data imputation for spectral audio signals. In *Proceedings of the IEEE International Workshop on Machine Learning for Signal Processing*, pages 1–6, Sep. 2009.
- [27] Shristi Rajbamshi, Georg Tauböck, Nicki Holighaus, and Peter Balazs. Audio inpainting via l1-minimization and dictionary learning. In *Proceedings of the 29th European Signal Processing Conference (EUSIPCO)*, pages 2149–2153, Dublin, Ireland, Aug. 2021. IEEE.
- [28] Ondřej Mokřý, Paul Magron, Thomas Oberlin, and Cédric Févotte. Algorithms for audio inpainting based on probabilistic nonnegative matrix factorization. *Signal Process.*, May 2023.
- [29] Mathieu Lagrange, Sylvain Marchand, and Jean-Bernard Rault. Long interpolation of audio signals using linear prediction in sinusoidal modeling. *J. Audio Eng. Soc.*, 53(10):891–905, Oct. 2005.
- [30] Nathanael Perraudin, Nicki Holighaus, Piotr Majdak, and Peter Balazs. Inpainting of long audio segments with similarity graphs. *IEEE/ACM Trans. Audio Speech Lang. Process.*, 26(6):1083–1094, 2018.
- [31] G. Greshler, T. Shaham, and T. Michaeli. Catch-a-waveform: Learning to generate audio from a single short example. In *Proceedings of NeurIPS*, volume 34, pages 20916–20928, Dec. 2021.
- [32] Bong-Ki Lee and Joon-Hyuk Chang. Packet loss concealment based on deep neural networks for digital speech transmission. *IEEE/ACM Trans. Audio Speech Lang. Process.*, 24(2):378–387, 2015.
- [33] Ju Lin, Yun Wang, Kaustubh Kalgaonkar, Gil Keren, Didi Zhang, and Christian Fuegen. A time-domain convolutional recurrent network for packet loss concealment. In *Proceedings of the IEEE International Conference on Acoustics, Speech and Signal Processing (ICASSP)*, pages 7148–7152. IEEE, May 2021.
- [34] Santiago Pascual, Joan Serrà, and Jordi Pons. Adversarial auto-encoding for packet loss concealment. In *Proceedings of the IEEE Workshop on Applications of Signal Processing to Audio and Acoustics (WASPAA)*, pages 71–75. IEEE, Oct. 2021.
- [35] Linlin Ou and Yuanping Chen. Concealing audio packet loss using frequency-consistent generative adversarial networks. In *Proceedings of the 5th International Conference on Pattern Recognition and Artificial Intelligence (PRAI)*, pages 826–831, Paris, France, May 2022. IEEE.
- [36] Giovanni Morrone, Daniel Michelsanti, Zheng-Hua Tan, and Jesper Jensen. Audio-visual speech inpainting with deep learning. In *Proceedings of the IEEE International Conference on Acoustics, Speech and Signal Processing (ICASSP)*, pages 6653–6657. IEEE, Jun. 2021.
- [37] Kin Wai Cheuk, Ryosuke Sawata, Toshimitsu Uesaka, Naoki Murata, Naoya Takahashi, Shusuke Takahashi, Dorien Herremans, and Yuki Mitsufuji. Diffroll: Diffusion-based generative music transcription with unsupervised pretraining capability. *arXiv preprint*, Oct. 2022.
- [38] Zalán Borsos, Matt Sharifi, and Marco Tagliasacchi. Speechpainter: Text-conditioned speech inpainting. In *Proceedings of INTERSPEECH*, Sep. 2022.
- [39] Yuancheng Wang, Zeqian Ju, Xu Tan, Lei He, Zhizheng Wu, Jiang Bian, and Sheng Zhao. Audit: Audio editing by following instructions with latent diffusion models. *arXiv preprint arXiv:2304.00830*, 2023.
- [40] Yinhuai Wang, Jiwen Yu, and Jian Zhang. Zero-shot image restoration using denoising diffusion null-space model. In *Proceedings of the International Conference on Learning Representations (ICLR)*, May 2022.
- [41] A. Lugmayr, M. Danelljan, A. Romero, et al. Repaint: Inpainting using denoising diffusion probabilistic models. In *Proceedings of the IEEE/CVF Conference on Computer Vision and Pattern Recognition*, pages 11461–11471, Jun. 2022.
- [42] Jiaming Song, Arash Vahdat, Morteza Mardani, and Jan Kautz. Pseudoinverse-guided diffusion models for inverse problems. In *Proceedings of the International Conference on Learning Representations (ICLR)*, May 2022.
- [43] Prafulla Dhariwal and Alexander Nichol. Diffusion models beat gans on image synthesis. In *Proceedings of NeurIPS*, volume 34, pages 8780–8794, Dec. 2021.
- [44] Tero Karras, Samuli Laine, Miika Aittala, Janne Hellsten, Jaakko Lehtinen, and Timo Aila. Analyzing and improving the image quality of stylegan. In *Proceedings of the IEEE/CVF Conference on Computer Vision and Pattern Recognition*, pages 8110–8119, Jun. 2020.

- [45] Zhifeng Kong, Wei Ping, Jiaji Huang, Kexin Zhao, and Bryan Catanzaro. Diffwave: A versatile diffusion model for audio synthesis. In *Proceedings of the International Conference on Learning Representations (ICLR)*, May 2021.
- [46] Julius Richter, Simon Welker, Jean-Marie Lemerrier, Bunlong Lay, and Timo Gerkmann. Speech enhancement and dereverberation with diffusion-based generative models. *arXiv preprint*, Aug. 2022.
- [47] Jonathan Ho, Tim Salimans, Alexey Gritsenko, William Chan, Mohammad Norouzi, and David J Fleet. Video diffusion models. In *Proceedings of NeurIPS*, Dec. 2022.
- [48] Tero Karras, Miika Aittala, Timo Aila, and Samuli Laine. Elucidating the design space of diffusion-based generative models. In *Proceedings of NeurIPS*, Dec. 2022.
- [49] Aapo Hyvärinen and Peter Dayan. Estimation of non-normalized statistical models by score matching. *J. Mach. Learn. Res.*, 6(4):695–709, Dec. 2005.
- [50] Heeseung Kim, Sungwon Kim, and Sungroh Yoon. Guided-tts: A diffusion model for text-to-speech via classifier guidance. In *Proceedings of the 39th International Conference on Machine Learning*, Jul. 2022.
- [51] Hyungjin Chung, Byeongsu Sim, Dohoon Ryu, and Jong Chul Ye. Improving diffusion models for inverse problems using manifold constraints. In *Proceedings of NeurIPS*, Dec. 2022.
- [52] Gino Angelo Velasco, Nicki Holighaus, Monika Dörfler, and Thomas Grill. Constructing an invertible constant-q transform with non-stationary gabor frames. In *Proceedings of the International Conference on Digital Audio Effects (DAFX)*, Paris, France, Sep. 2011.
- [53] Nicki Holighaus, Monika Dörfler, Gino Angelo Velasco, and Thomas Grill. A framework for invertible, real-time constant-q transforms. *IEEE Trans. Audio Speech Lang. Process.*, 21(4):775–785, Apr. 2012.
- [54] Christian Schörkhuber and Anssi Klapuri. Constant-q transform toolbox for music processing. In *Proceedings of the 7th Sound and Music Computing Conference*, pages 3–64, Barcelona, Spain, 2010.
- [55] Christian Schörkhuber, Anssi Klapuri, and Alois Sontacchi. Pitch shifting of audio signals using the constant-q transform. In *Proceedings of the International Conference on Digital Audio Effects (DAFx)*, Jul. 2012.
- [56] Olaf Ronneberger, Philipp Fischer, and Thomas Brox. U-net: Convolutional networks for biomedical image segmentation. In *Proceedings of the International Conference on Medical Image Computing and Computer-Assisted Intervention*, pages 234–241. Springer, Nov. 2015.
- [57] Haibin Wu, Ke Tan, Buye Xu, Anurag Kumar, and Daniel Wong. Rethinking complex-valued deep neural networks for monaural speech enhancement. In *Proceedings of INTERSPEECH*, Jan. 2023.
- [58] Matthew Tancik, Pratul Srinivasan, Ben Mildenhall, Sara Fridovich-Keil, Nithin Raghavan, Utkarsh Singhal, Ravi Ramamoorthi, Jonathan Barron, and Ren Ng. Fourier features let networks learn high frequency functions in low dimensional domains. In *Proceedings of NeurIPS*, volume 33, pages 7537–7547, Dec. 2020.
- [59] Ethan Perez, Florian Strub, Harm De Vries, Vincent Dumoulin, and Aaron Courville. Film: Visual reasoning with a general conditioning layer. In *Proceedings of the AAAI Conference on Artificial Intelligence*, volume 32, Mar. 2018.
- [60] Md Amirul Islam, Sen Jia, and Neil DB Bruce. How much position information do convolutional neural networks encode? In *Proceedings International Conference on Learning Representations (ICLR)*, May 2020.
- [61] Ashish Vaswani, Noam Shazeer, Niki Parmar, Jakob Uszkoreit, Llion Jones, Aidan N Gomez, Łukasz Kaiser, and Illia Polosukhin. Attention is all you need. In *Proceedings of NeurIPS*, volume 30, Dec. 2017.
- [62] A. Gray and J. Markel. Distance measures for speech processing. *IEEE Trans. Acoustics, Speech, Signal Process.*, 24(5):380–391, 1976.
- [63] Rainer Huber and Birger Kollmeier. Pemo-q—a new method for objective audio quality assessment using a model of auditory perception. *IEEE Trans. Audio Speech Lang. Process.*, 14(6):1902–1911, Nov. 2006.
- [64] Kevin Kilgour, Mauricio Zuluaga, Dominik Roblek, and Matthew Sharifi. Fréchet audio distance: A reference-free metric for evaluating music enhancement algorithms. In *Proceedings of INTERSPEECH*, pages 2350–2354, Sep. 2019.
- [65] John Thickstun, Zaid Harchaoui, and Sham Kakade. Learning features of music from scratch. In *Proceedings International Conference on Learning Representations (ICLR)*, May 2016.
- [66] ITU. Method for the subjective assessment of intermediate quality level of audio systems. Rec. BS.1534-3, International Telecommunication Union, Geneva, Switzerland, October 2015.
- [67] Michael Schoeffler, Sarah Bartoschek, Fabian-Robert Stöter, Marlene Roess, Susanne Westphal, Bernd Edler, and Jürgen Herre. WebMUSHRA—A comprehensive framework for web-based listening tests. *J. Open Res. Softw.*, 6(1):1–8, Feb. 2018.